Noname manuscript No.
(will be inserted by the editor)

A fast image dehazing method that does not introduce color artifacts

Javier Vazquez-Corral · Adrian Galdran · Praveen Cyriac · Marcelo Bertalmío

Received: date / Accepted: date

Abstract We propose a method for color dehazing with four main characteristics: it does not introduce color artifacts, it does not depend on inverting any physical equation, it is based on models of visual perception, and it is fast, potentially real-time. Our method converts the original input image to the HSV color space and works in the saturation and value domains by: i) reducing the value component via a global constrained histogram flattening, ii) modifying the saturation component in consistency with the previous reduced value, and iii) performing a local contrast enhancement in the value component. Results show that our method competes with the state-of-the-art when dealing with standard hazy images, and outperforms it when dealing with challenging haze cases. Furthermore, our method is able to dehaze a FullHD image on a GPU in 90 milliseconds.

Keywords Image dehazing · Color image processing · Vision models

1 Introduction

Atmospheric phenomena such as fog or haze tend to scatter light, often degrading the visual quality of images acquired outdoors. Objects that are further away appear to vanish or melt into the horizon. Kochsmieder [24] modeled this effect as directly proportional to the distance of the object from the observer, and proposed the following light propagation law:

$$\mathrm{I}(x) = \mathrm{t}(x)\mathrm{J}(x) + (1 - \mathrm{t}(x))\mathrm{A}, \tag{1}$$

J. Vazquez-Corral, P. Cyriac and M. Bertalmío
Department of Information and Communications Technologies
Universitat Pompeu Fabra
E-mail: javier.vazquez,praveen.cyriac,marcelo.bertalmio@upf.edu

A. Galdran
INESC TEC, R. Dr. Roberto Frias, 4200 Porto (Portugal)
E-mail: adrian.galdran@inesctec.pt

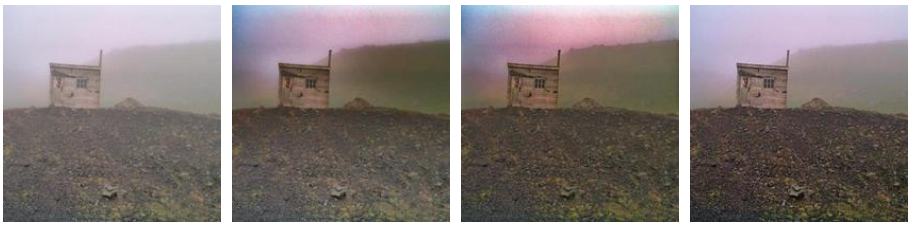

(a) **(b)** **(c)** **(d)**

Fig. 1: *An example of artifacts appearing in current image dehazing methods. a) Original image b) He* et al. *[21], c) Meng* et al. *[33], d) our result.*

where in terms of image processing, x represents a pixel location, $\mathrm{I}(x)$ is the intensity captured by detectors within the camera, $\mathrm{J}(x)$ is the radiance in a hypothetical haze-free scene, $\mathrm{t}(x)$ is the transmission of light in the atmosphere, inversely related to the scene's depth, and A is the airlight, a vector quantity describing the predominant color of the atmosphere.

Most outdoor computer vision systems, performing for instance tracking or surveillance, assume images acquired under good weather conditions. In such scenario, no scattering happens, i.e. $\mathrm{t}(x) \equiv 1$, and the image corresponds to the scene radiance, $\mathrm{I}(x) = \mathrm{J}(x)$. However, the assumption that the section of atmosphere lying in between the camera and the objects is completely transparent is often not realistic. The task of removing that degradation produced by the atmosphere is known as image dehazing.

A great progress has been achieved in recent years towards the goal of effectively eliminating haze or fog from images. Several different general approaches have appeared (see *Related Work* below), but the predominant strategy is to try to recover the radiance $\mathrm{J}(x)$ from the acquired intensity through inversion of the physical model in Eq. (1). This requires first to estimate the haze distribution across the scene, which should be inversely related to transmission $\mathrm{t}(x)$, and also the airlight illuminant A . Once estimates for $\mathrm{t}(x)$ and A are available, a clean image is readily obtained by inverting Eq. (1):

$$\mathrm{J}(x) \approx \frac{\mathrm{I}(x) - \mathrm{A}(1 - \mathrm{t}(x))}{\mathrm{t}(x)}. \tag{2}$$

Unfortunately, the physical model described in Eq. (1) assumes that no noise is captured by the imaging device. As discussed in [32], if we consider an extended model incorporating noise $\eta(x)$:

$$\mathrm{I}(x) = \mathrm{t}(x)\mathrm{J}(x) + (1 - \mathrm{t}(x))\mathrm{A} + \eta(x), \tag{3}$$

the resulting solution is:

$$\mathrm{J}(x) \approx \frac{\mathrm{I}(x) - \mathrm{A}(1 - \mathrm{t}(x))}{\mathrm{t}(x)} - \frac{\eta(x)}{\mathrm{t}(x)}. \tag{4}$$

Since transmission $\mathrm{t}(x)$ varies in $[0, 1]$, and it is inversely related to depth in the scene, we can conclude that in far away areas of the scene, noise will be strongly amplified. This problem is exacerbated by the limitation that $\mathrm{t}(x)$ is a scalar quantity describing at the same time the propagation of light in the different chromatic components. This unavoidably leads

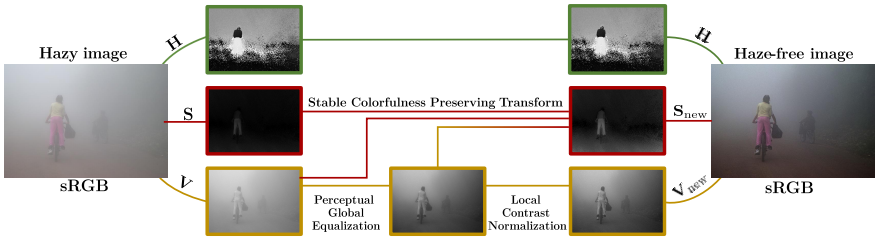

Fig. 2: *The pipeline of our method.*

to the appearance of color artifacts in such situations, and is also the reason why most of current dehazing approaches find it difficult to deal with images containing sky regions.

This limitation may sometimes lead to a dehazed output of inferior quality than the original image. We can visually verify the above observations in Figure 1, where we show the original image and the result of two state-of-the-art methods: He *et al.* [21] and Meng *et al.* [33]. The output of the method developed in this paper is also introduced for comparison.

The main contribution of this paper is therefore the proposal of a new image dehazing technique that, rather than neglecting the presence of noise, attempts to recover a haze-free image while reducing the disturbing chromatic artifacts typical of current approaches. The proposed method operates in the HSV color space, and has the following features:

1. It does not introduce color artifacts, *by-design*.
2. It is based in vision science models and natural image statistics.
3. It does not depend on inverting any physical equation.
4. Its computational complexity is very low.

More in detail, we start by performing in the Value component a global transform aiming to flatten its histogram. This global function is based on the statistics of natural scenes [12]. Next, we modify the Saturation component in order to keep the colorfulness of the scene. This modification follows the ideas suggested in [36, 37] where authors state that stable colorfulness may be a human color cue in hazy scenes. Finally, we perform local contrast enhancement on the Value component based on contrast normalization [7, 9] in the retina and following the principles of efficient coding [22]. Our proposed method only depends on two straightforward parameters that can be tuned depending on whether the user wants a saturated result and on whether the user wants a lower or higher contrast enhancement, considering that some noise may appear when this parameter is too large. Therefore, our method has a mechanism to control the magnification of noise or even blocking artifacts when they are already present in the original image. A pipeline of the method is presented in Figure 2.

The resulting technique is simple, robust to chromatic noise and potentially real-time. Therefore, its reliability and efficiency makes it suitable to be introduced as a style option in any digital camera. Furthermore, its GPU implementation only takes 90 milliseconds to dehaze a FullHD image.

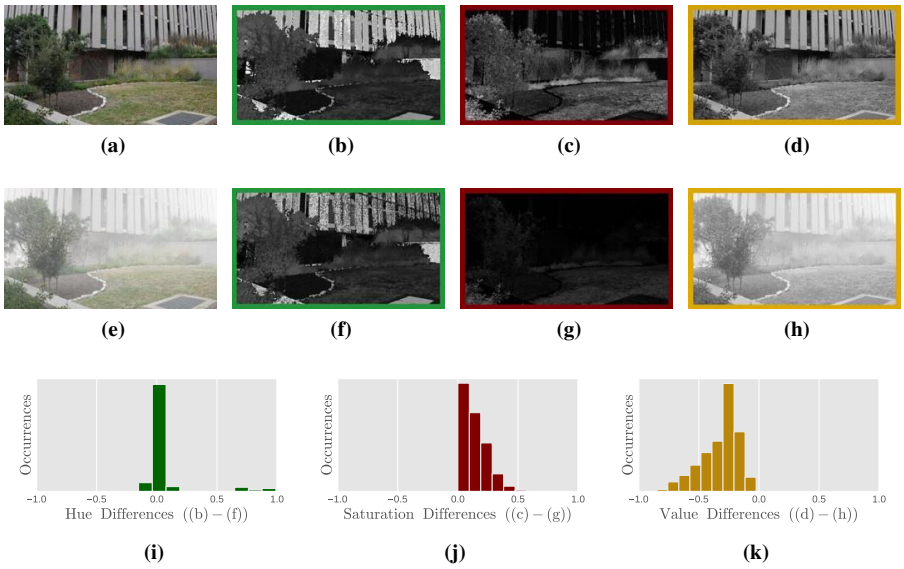

Fig. 3: *Comparison between a fog and a non-fog image in the HSV space. First two rows, from left to right: Original image, hue, saturation and value. Last row: Histogram of differences between the fog and the non-fog image. We can see that hue stays the same, while saturation is always higher for the non-fog image, and value is always higher for the fog image.*

2 Related work

Many methods have appeared in the last years that attempt to remove fog from a weather-degraded outdoor image. While the goal of all of these techniques is to enhance the visibility of the input image, there are several substantially different ways to attack this problem. Here, we divide these approaches into three categories: a) Physically-based methods, b) Machine Learning methods, and c) Advanced Image Processing methods.

Physically-based methods: These are methods that attempt to solve for the haze-free image $\mathrm{J}(x)$ in Eq. (1). Since inverting Eq. (1) poses an underdetermined problem, this requires either to consider some kind of external extra information source or to make additional assumptions on the model to constrain the space of possible solutions. Related to the former possibility, there exist several methods that require several images captured in different conditions [23, 38, 44, 45]. When no extra information apart from the input image is considered, the problem is usually referred to as single-image dehazing. The typical approach in this case is to formulate some kind of restriction on the visual characteristics that a reasonable solution can have. Examples of this category are [14], [39], or [50]. Probably the most popular technique in this category is the Dark Channel prior [21]. Much research on image dehazing is based on this statistical cue, attempting to extend it in several directions to improve it or make it more robust, see [19, 25, 28, 33, 46, 55, 63] for recent contributions in this

direction. Finally, some other works combine the dark-channel cue with an extra correction on the HSV color space, e.g. see [54] and [61].

Machine-learning approaches: These techniques are based on the incorporation of prior knowledge, obtained from statistical observations of visual features on datasets of human-labeled foggy and fog-free images. For instance, in [48] the authors study several haze-relevant features, in order to establish a combination useful to learn a haze-removal regression model. The method in [63] learns a linear model of depth instead of a model of hazy and haze-free images. To obtain depth map examples on which to train, the authors generate synthetic depth images following the strategy outlined in [48]. The same approach has been recently employed in order to generate enough examples to train a deep convolutional neural network in [8]. Another interesting approach is that of [63], where the authors consider the color attenuation prior. This prior assumes that in haze-free images the difference between the saturation and the value components of the HSV correlates with the amount of haze present in the scene. Also recently, a haze density predictor based on natural scene statistics has been presented in [11]. After collecting a series of haze-relevant statistical features, a haze-density map is computed by analyzing the Mahalanobis distance of the hazy input features and the corresponding features of a dataset of haze-free images. Moreover, this approach can also be used to defog hazy images. Recently, Luan *et al.* [30] propose to study 7 different haze-relevant features based on image quality, and to learn a regression from these features to obtain the transmission map.

Advanced image processing approaches: Although these methods are usually partly based on a model such as the one in Eq. (1), they also rely in advanced spatially varying image processing techniques. These approaches often study the local structure of the image, in terms of the amount of contrast, saturation or other possible indicators of the presence of haze, and try to compensate for this effect. For instance, the method in [47] is based on three observations, namely: a haze-free image contains more local contrast than a hazy one, the amount of haze in a region varies smoothly, and nearby pixels are usually located in the same depth layer of the scene, i.e., they are equally affected by haze. These observations are modeled through a cost function, the minimization of which maximizes contrast while preserving depth smoothness, to yield a clean image. In [40] the authors propose a method to remove contrast loss in hazy images through a linear model of the presence of excessive brightness, based on the ratio between local mean and standard deviation. More recently, in [1, 2] the authors use a multiscale image fusion approach in which they blend several images derived from the input, such as a white-balanced and a contrast-enhanced version of it. Approaches based on models of the Human Visual System, such as Retinex, have also been proposed in [16–18, 53, 60, 62]. Recently, Wang *et al.* [59] propose that a linear relationship exists in the minimum channel between the hazy image and the haze-free image, and they consider this relationship to obtain haze-free images.

Still related to this set of approaches, the method proposed by Wang *et al.* [56] is the closest to our approach. In [56] authors propose to perform a local content-adaptative histogram equalization on the intensity followed by a saturation modification that depends on the intensity contrast. Our approach follows a similar scheme, with the following main differences: i) our approach performs a global histogram equalization in the Value component following visual science results to avoid the appearance of artifacts [41], and ii) our modification of the saturation is constrained to not modify the chroma of the original scene, following

again the vision science literature [36, 37]. Finally, our model optionally performs a local enhancement only as a last step. All these differences allow our method to be two orders of magnitude faster than [56] already with the non-optimized Matlab version of our code. Let us remark that our approach also provides more pleasant results and it is better than that of Wang *et al.* as computed using several metrics, as we demonstrate in the Results section.

Remarkably, very few methods have addressed the need of removing artifacts while dehazing a degraded image. Matlin *et al.* [32] proposed to perform simultaneous denoising and dehazing using an iterative, adaptive, non-parametric regression method. Li *et al.* [26] introduced a contrast enhancement method that decomposes the image into high and low frequencies, performing the enhancement only in the low frequencies, thus avoiding blocking artifacts. Also, Chen *et al.* [10] present a visual artifact suppression method for dehazing by applying both a smoothing filter for the refinement of the transition and an energy minimization in the recovery phase to avoid the appearance of gradients in the output image that were not presented in the original image. Recently, Wang *et al.* [58] proposed to consider the quad-tree method to perform a region decomposition. Then, based on this region decomposition, the authors propose a method that does not present artifacts in the sky region.

Finally, very few real-time methods have been designed for the image and video dehazing problem, e.g. [4], [13]. These two approaches are based on the Dark Channel Prior, where [4] optimizes the medium transmission using a guided filter while [13] considers an optimized reconstruction formula and operates in a multi-scale resolution. In both cases, the optimization proposed results in an image of reduced quality when compared to the original Dark Channel Method [21].

3 Joint global and local dehazing in the HSV space

The proposed technique is composed of five different stages. First, the original hazy image is converted to the HSV color space. Second, we modify the Value component $V(x)$, where x denotes a particular pixel, by means of a global histogram equalization, but constrained by some perceptually-inspired assumptions. The modified Value component $V_{global}(x)$ is then employed to modify the Saturation component $S(x)$ in such a way that the colorfulness of the output resembles the colorfulness of the original image. After $S(x)$ has been modified, we enhance again the Value component, this time through a local contrast operation that is related to the contrast normalization process of the visual system. Finally, we map the processed image back to the sRGB space, obtaining a haze-free version of the original hazy input. In the rest of this section, we explain in detail every step of the method.

3.1 Conversion to the HSV color space

Hue, Saturation and Value (HSV) color space is a cylindrical color space widely used in computer vision and image processing. It separates the color information of an image into the dye of the color (hue component), the brightness of the color (value component), and the intensity of the color related to an achromatic one (saturation component). Mathematically, we can convert any sRGB color image into the HSV color space by a set of well defined formulas (see Appendix).

In Figure 3 we present an original haze-free image and the same image with a synthetic fog layer on top of it. This haze layer has been simulated following the model proposed in [52]. The corresponding H, S, and V channels of both images are shown in the first two rows, and the histogram of their differences is displayed in the third row. Note that the Hue component is circular and normalized between 0 and 1. Therefore, two pixels that lie within a distance of 1 in this representation contain the same amount of hue. By looking at the figure we can observe that in the HSV space, performing image dehazing amounts to increasing the Saturation and decreasing the Value components, while leaving the Hue component unaltered. For this reason, once the image is converted to the HSV space, our method only modifies the Saturation and Value of the input hazy image.

3.2 Perceptually-based global constrained histogram equalization

From Figure 3, we can see that the Value difference is always negative. This indicates that the histogram of the V component of a hazy image is typically skewed towards 1. Distributing these values uniformly across the available dynamic range should thus contribute to increase contrast and detail visibility in the image.

In [12], the authors proposed an adaptive non-linear transform that performs a histogram equalization on an image I, subject to different perceptually inspired constraints. This transform is formulated to be consistent with the efficient coding hypothesis, *e.g.*, that the Human Visual System uniformly distributes the input signal when presented with natural scenes [41]. The slope function γ that determines the non-linearity of this transform, based on natural image statistics, is computed as follows:

$$\gamma(I(x)) = \gamma_H + (\gamma_L - \gamma_H)\left(1 - \frac{I(x)^n}{I(x)^n + M_{lin}^n}\right), \tag{5}$$

where x is an image pixel. Here, the parameters γ_L, γ_H, and M can be estimated from the cumulative histogram of the intensity image in log-log coordinates, see [12]; M_{lin} denotes the exponential of M (since M is computed from log-luminance values), and n is a fixed exponent that regulates the steepness of the curve (in practice, $n = \gamma_L$). The function γ models this way the non-linearity as a smooth curve that approximates the cumulative histogram. The parameter γ_L is replaced by 1.1 in case it is bigger than this value.

Let us note that the model in [12] expects a linear image as input. Therefore, we first need to linearize the Value component of the input hazy image V_{in} by applying the inverse of encoding gamma to obtain $V_{in}^l = V_{in}^{2.2}$. Once this correction is applied, we employ Eq. (5) to perform a constrained histogram equalization on V_{in}^l:

$$V_{global}(x) = (V_{in}^l(x))^{\gamma(V_{in}^l(x))}. \tag{6}$$

3.3 Saturation modification through stable colorfulness

In [36, 37] the authors state that human observers are able to perceive the same level of colorfulness independently from the quantity of haze present in the scene. In the HSV color space, a measure related to colorfulness is the $Chroma_{HSV}$, which is defined by

the product of Saturation by Value. Note that $Chroma_{HSV} = S \times V$ is different from $Chroma_{ab} = \sqrt{a^2 + b^2}$, since in HSV the Value has an influence in the chroma, while in Lab the Luminance has no influence.

According to the above observation, our goal is then to modify the Saturation component while respecting as much as possible the $Chroma_{HSV}$. This implies modifying the Saturation component, but incorporating the global Value modification performed in section 3.2 Since $Chroma_{HSV} = S \times V$, we propose the following modification for the Saturation component:

$$S_{new}(x) = \left(\frac{V_{in}(x)}{V_{global}(x)} S_{in}(x) \right)^{\tau}, \tag{7}$$

where in this equation we have introduced a power value of τ in order to avoid obtaining a colorfulness smaller than the original (as we still need to apply the last stage of our method consisting on a local value modification, which can further reduce the Value component). Let us note that, in the case of considering a power value of $\tau = 1$, the $Chroma_{HSV}$ component of the dehazed image at this stage would be the same as the original, and if we decreased the power value, $Chroma_{HSV}$ of the dehazed image would increase. An analysis of the behaviour of τ is presented in section 4.1. As explained there, in all the results of this paper we use $\tau \in [0.7 - 0.8]$, as smaller values over-saturate the image and bigger values are not able to recover enough saturation of the colors.

3.4 Contrast normalization for local value enhancement

The global non-linear transform performed by Eq. (6) may not be able to completely preserve the local contrast in the Value component, leading to a loss of image detail. As a result, in [12] the authors subsequently applied a local contrast normalization. This operation is modeled after findings from the neuroscience literature (see [7, 9, 22] and references therein), that show that the human visual system implements a mechanism called contrast normalization, by which the local contrast of a scene is normalized by a factor depending on the standard deviation of the incoming light intensity.

Here, we follow the same approach and apply local contrast normalization on the Value component, according to the following formula:

$$V_{new}(x) = \mu(x) + (V_{global}(x) - \mu(x)) \cdot \frac{k}{\sigma}, \tag{8}$$

where x is a pixel, $\mu(x)$ is the local mean of V_{global}, σ is the standard deviation of V_{global}, and k is a constant that accounts for the desired level of contrast. The standard deviation is replaced by 0.25 in case it is smaller than this value.

3.5 Back-conversion to the sRGB space

The remaining step consists of converting the processed image back to sRGB. As in the first subsection, there is a set of well defined formulas (see Appendix) to achieve this. Let us note that the processed image consists of the original Hue H_{in}, and the modified versions of the Saturation S_{new} and the Value V_{new} components.

Algorithm 1 Proposed method

Input: $sRGB$ hazy image.
1. Convert the input image from sRGB to HSV. Denote the three new channels as V_{in}, H_{in} and S_{in}.
2. Compute $V_{in}^{l} = V_{in}^{2.2}$.
3. Compute the cumulative histogram of V_{in}^{l} to obtain $M_{lin}, \gamma_L, \gamma_H$ following [12].
4. Compute $\gamma(V_{in}^{l}(x)) = \gamma_H + (\gamma_L - \gamma_H)\left(1 - \frac{(V_{in}^{l}(x))^n}{(V_{in}^{l}(x))^n + M_{lin}^n}\right)$.
5. Compute $V_{global}(x) = (V_{in}^{l}(x))^{\gamma(V_{in}^{l}(x))}$.
6. Compute $S_{new}(x) = \left(\frac{V_{in}(x)}{V_{global}(x)} S_{in}(x)\right)^{\tau}$.
7. Compute $V_{new}(x) = \mu(x) + (V_{global}(x) - \mu(x)) \cdot \frac{k}{\sigma}$, where $\mu(x)$ is the local mean and σ the standard deviation of V_{global}.
8. Convert the image composed by H_{in},V_{new}, and S_{new} back to sRGB.
Result: $sRGB$ dehazed image.

3.6 Summary of our approach

An algorithmic summary of our method is presented in Algorithm 1. All the operations of our method have very low computational complexity and can potentially be implemented in-camera. Let us discuss this in detail. Operations **1.** and **8.** of the algorithm are simply color conversions, and can be approximated by look-up-tables (LUTs). Operation **2.** is a pixel-based power function that can also be stored as a LUT. Operation **3.** just needs to compute the cumulative histogram of the value component to obtain the set of parameters. Operations **4. and 5.** are the definition and application of a non-linear transform. This step can be costly if it is not properly programmed. For this reason we define γ as a LUT by evaluating the equation of Operation **4.** (i.e. Eq. 5 in the paper) at equal intervals in the range $[0 - 1]$, and then Operation **5.** is just the execution of the LUT. Operation **6.** is a pixel-based modification composed of simple arithmetic operations and a power function. Again, we can conveniently approximate the power function with a LUT, as saturation values are always between 0 and 1. Finally, Operation **7.** is very similar to the unsharp masking process carried out in many camera models and can therefore be executed with low complexity. In particular, this last operation computes: i) the local mean of the image as a convolution, that in Fourier Space has a computational complexity of $o(n \log n)$), and ii) a pixel-wise linear operation. Let us also note that all the operations of our method can be easily parallelized.

4 Results

In this section we first perform an analysis of the main parameters of our method. Later we compare our method versus the state-of-the-art both qualitatively and quantitatively with non-reference and full-reference image metrics. Then, we present the psychophysical experiment that we designed for the comparison of the algorithms. We compare our approach to other artifact-aware methods, and finally we compare the computational time of the different approaches.

Fig. 4: *Analysis of the parameters of the approach. The first column shows the original image. In the rest of the figure, the parameter τ moves between 0.5 in the first row to 0.9 in the last row in equal increments. Column-wise we have the result of our method with $k = 0.3$ in the first column, $k = 0.5$ in the second column, and $k = 0.7$ in the last column.*

4.1 Analysis of the parameters

We start analyzing the effect of the parameters τ and k of our approach. Figure 4 shows the original image in the first column. Then, in the other three columns, we show different results of the method by modifying both k and τ. In particular, the value of k changes over the different columns in an increasing manner (from 0.3 in the second column to 0.5, and 0.7). Conversely, the value of τ is increased row-wise, (from 0.5 for the first row, to 0.7, and 0.9). Regarding the parameter k, we can observe that as its value increases, the local contrast increases. Regarding the parameter τ, as its value decreases the image presents more saturated colors, but when τ becomes too small the image loses realism due to the over-saturation. In general, indoor scenes usually present saturated man-made colors, while

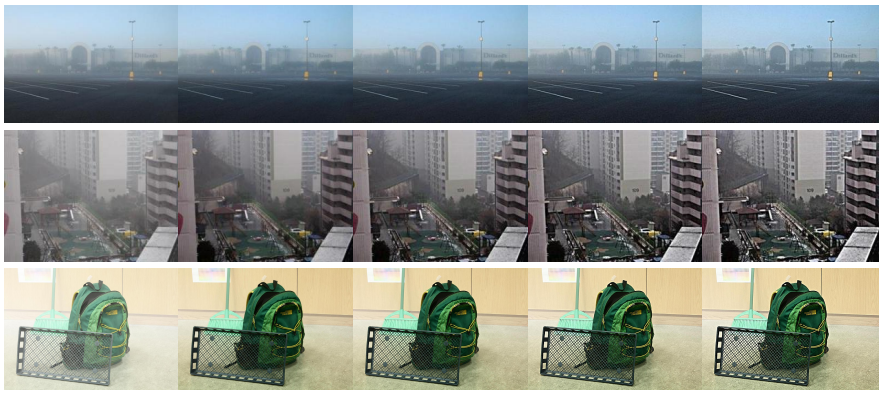

Fig. 5: *Analysis of the effect of parameter k. From left to right: Original hazy image, global part of our method (steps 1 to 6), the output of our full method with $k = 0.4$, $k = 0.6$, and $k = 0.8$.*

outdoor scenes present natural colors. For this reason we will use $\tau = 0.8$ for outdoor hazy scenes and $\tau = 0.7$ for indoor synthetic scenes in this paper.

Let us now focus more on the behaviors of the k parameter. In Figure 5 we compare the result produced with different k values, from left to right: hazy image, the output of the global part of our method (steps 1 to 6), the output of our full method with $k = 0.4$, $k = 0.6$, and $k = 0.8$. We can see in the first two rows that in the case of real outdoor hazy images as k increases more dehazing is achieved, but at the expense of a magnification of contrast, leading to some noise enhancement. Therefore, for outdoor scenes where faraway regions need to be restored a middle value of k of around 0.4 to 0.6 seems to be a good trade-off between dehazing power and perceived noise. On the other hand, in indoor scenes the objects are closer to the camera and therefore, there is no need for dehazing faraway regions. In this case, the global part of our method already provides good results, while bigger values of k excessively over-enhance the image.

4.2 Comparison versus state-of-the-art

Let us now qualitatively compare our results versus current state-of-the-art methods, namely those of Choi *et al.* [11], Meng *et al.* [33], Tarel *et al.* [51], the Dark-Channel (DC) [21], and Wang *et al.* [56].

We first consider some standard images in the dehazing literature. Results for these images are presented in Figure 6. In this figure we show (from left to right) the original image, Choi *et al.*, Dark-channel, Meng *et al.*, Tarel *et al.*, Wang *et al.*, and our results with $k = 0.4$, and $k = 0.6$. Our method is competitive with the rest of image dehazing methods for this set of standard haze images. In particular, let us remark the excessive saturation of the methods of Choi *et al.* in the second, fourth, and fifth image, the greysh cast in the method of Tarel *et al.*, and the excessive contrast in the fourth image for the method of Wang *et al.*. In particular, our method can compete in each of the scenes to the best result.

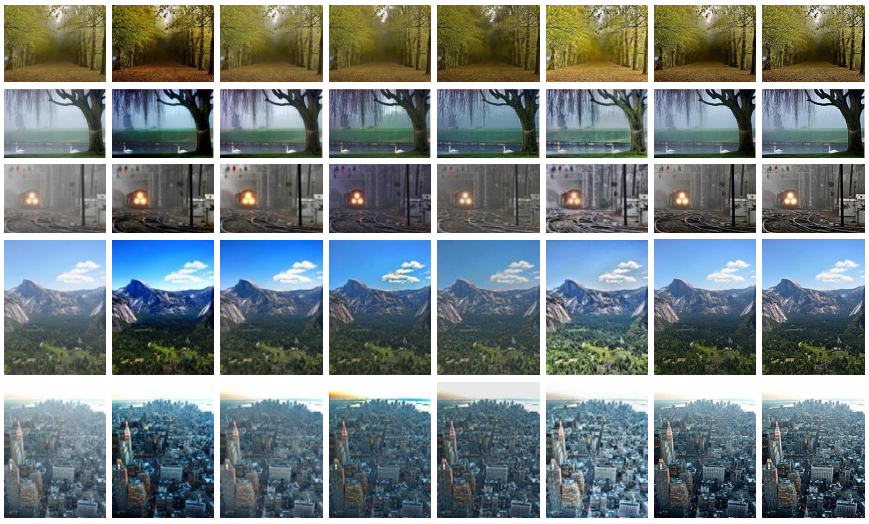

Fig. 6: *Results when dehazing standard images.*

The main advantage of our method is more apparent when challenging images are tested, like the ones in Figure 7. The order of presentation is the same as in the previous figure. In the images presented here, the artifacts that appear in the results of state-of-the-art methods are explicit. These artifacts are so prominent that the original image tends to be preferred over the dehazed result (focus for example on the fourth image for the case of Choi *et al.*, the third image for the case of Dark-Channel, the second image for Meng *et al.*, the fifth or sixth image for Tarel *et al.*, and the fifth, seventh, and eighth for Wang *et al.*). This last method over-saturates the green of the trees in the fifth image and it creates a very strange effect in the water in the last one, that looks completely unrealistic. In contrast, the results presented by our approach are dehazed without producing any artifact. Let us note that the work of Meng *et al.* performs both image dehazing and white balancing, due to their computation of the image locality, while the other methods suppose the haze color to have been already white-balanced.

Non-reference quantitative evaluation To quantitatively compare our results versus the state-of-the-art methods we use the FADE perceptual blind image quality metric [11], the e-score and the r-score metrics proposed by Hautière *et al.* in [20], and the BRISQUE [35] and NIQE [34] measures as proposed in Wang and Yuan [57]. FADE is pre-trained to look for measurable deviations between natural foggy and fog-free images and then uses these deviations to estimate the visibility of a foggy scene from a single image. The e-score and the r-score compute ratios at visible edges to analyze the improvement in their visibility. Finally, BRISQUE and NIQE are image quality metrics. FADE, NIQE and BRISQUE metrics do not use any other image apart from the one to be evaluated, while e-score and r-score need to be compared to the original hazy image, but not to a ground-truth. We run the metrics on a set of 600 foggy images presented in [11]. Results are shown in Table 1. We can see that for the FADE metric our method improves, as we increase the value k. Our method with

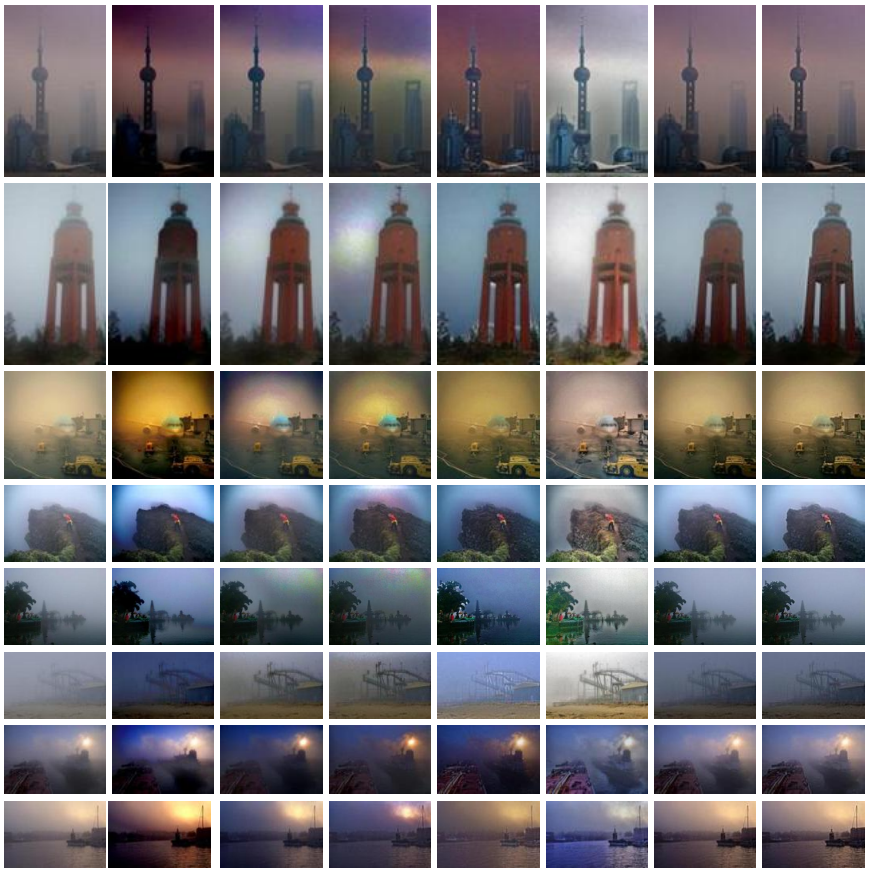

Fig. 7: *Results when dehazing challenging images.*

$k = 0.4$ is already competitive with state-of-the-art methods, and with $k = 0.6$ is second to Choi *et al.* according to the metric (let us remark here that Choi *et al.* method is designed to minimize this metric). Regarding the e-score the best methods are the ones of Tarel *et al.* and Meng *et al.*. On the r-score the best method is the one of Wang *et al.* followed by our method with $k = 0.6$. Our method with $k = 0.6$ ranks the best for the NIQE metric, followed by the one of Meng *et al.*, and for the BRISQUE dataset the best methods are the Dark-channel, the method from Tarel *et al.*, and our global method. Finally, let us note that all the images from Figures 6 and 7 are from the dataset used in this evaluation.

Full-reference quantitative evaluation We consider the Middlebury subset from the D-HAZY dataset [3] in order to compute a full-reference image metric on our results. In this dataset, for each scene we have a pair of fog/no-fog registered images that allows us to compute full-reference metrics between the result of the method applied to the fog image and the original no-fog image. We compute the results for the ΔE and the $SSIM$ metrics as suggested in [3] for all the methods used before, and we also add the results for the CLAHE [43],

Table 1: *Non-reference quantitative results for the different methods on the 600 foggy images of the FADE dataset using different metrics. Best result is marked in green, second-best in blue, and third-best in orange; med. stands for median, trim. stands for trimean.*

	FADE		e-score		r-score		NIQE		BRISQUE	
	med.	trim.	med.	trim.	med.	trim.	med.	trim.	med.	trim.
Choi *et al.*	**0.42**	**0.44**	0.34	0.40	1.45	1.44	4.04	4.04	**18.75**	**19.01**
Meng *et al.*	0.49	0.50	**0.63**	**0.72**	1.79	**1.85**	**3.65**	**3.68**	21.75	22.26
Tarel *et al.*	0.48	0.54	**0.79**	**0.63**	**1.88**	1.82	4.29	4.30	27.20	28.03
Dark-channel	0.83	0.85	0.16	0.21	1.04	1.07	3.90	3.90	**15.25**	**15.44**
Wang *et al.*	**0.47**	**0.49**	**0.53**	**0.63**	**2.95**	**2.96**	3.85	3.84	24.99	25.99
Ours-only global	0.90	0.94	0.14	0.17	1.14	1.14	**3.72**	3.76	**21.29**	**21.75**
Ours-$k = 0.4$	0.64	0.67	0.29	0.35	1.62	1.63	3.76	**3.74**	22.84	23.06
Ours-$k = 0.6$	**0.45**	**0.47**	0.38	0.46	**2.19**	**2.20**	**3.53**	**3.54**	23.51	24.24

Fig. 8: *Results for images in the Middleburry part of the D-Hazy dataset.*

Ancuti and Ancuti [1], and Fattal [15] methods given in [3]. Also, we compute the CID metric [29] for those methods compared in the non-reference case. CID is a color extension of the SSIM metric that looks for the changes, from one image to the other, in features such as hue, lightness, chroma, contrast, and structure.

Results are shown in Table 2. We can see that Dark Channel provides the best results in this case. Our global method ranks five times as second and one time as third, while our method with $k = 0.4$ ranks three times as third. Let us note here that the foggy images in this dataset are created from well-exposed indoor no-foggy images, and therefore, the dark-channel hypothesis is mostly-accomplished by design in all the cases.

In Figure 8 we compare the results of the different methods for three of the images in the dataset. From left to right: the ground-truth image, the hazy input image, Choi *et al.*, Dark-channel, Meng *et al.*, Tarel *et al.*, Wang *et al.*, our global result, and our result with $k = 0.4$. We can clearly see that Choi *et al.* makes the image too dark, Meng *et al.* gives a bluish cast for the first and over-saturates the color for the second image, while Wang *et al.*, and Tarel *et al.* wash-out the colors of the image. The method of Wang *et al.* also over-increases the contrast creating unrealistic results. The dark-channel method is the closer to the ground-truth for the three images, although it introduces some artifacts in the last one. Our method does not introduce artifacts, although it still misses some extra saturation.

	CID		Delta E		SSIM	
	median	trimean	median	trimean	median	trimean
Original	0.61	0.59	22.86	24.09	0.77	0.78
Tarel *et al.*	0.45	0.43	15.86	16.18	0.83	0.82
Choi *et al.*	0.58	0.57	19.76	20.54	0.74	0.74
Meng *et al.*	0.43	0.43	14.12	14.07	**0.85**	**0.84**
Dark Channel	**0.33**	**0.33**	**10.05**	**10.72**	**0.88**	**0.88**
CLAHE	-	-	14.78	14.91	0.68	0.67
Ancuti and Ancuti	-	-	13.26	**13.69**	0.84	**0.84**
Fattal	-	-	16.06	16.34	0.80	0.81
Wang *et al.*	0.54	0.52	15.93	16.44	0.82	0.81
Ours-only global	**0.38**	**0.41**	**12.57**	**13.90**	**0.85**	**0.85**
Ours-$k = 0.4$	**0.42**	**0.42**	**12.69**	13.97	0.83	0.83

Table 2: *Full-reference quantitative results for the different methods on the Middleburry set of the D-Hazy dataset. Best result is marked in green, second-best in blue, and third-best in orange*

4.3 Psychophysical evaluation

We have also performed a psychophysical experiment and details are given below.

4.3.1 Subjects

Fifteen subjects completed the experiment. Two are authors of the paper. All observers were tested for normal color vision using the Ishihara color blindness test. Ethics was approved by the Comité Etico de Investigacion Clinica, Parc de Salut MAR, Barcelona, Spain and all procedures complied with the declaration of Helsinki.

4.3.2 Apparatus

Experiment was conducted on an AOC I2781FH LCD monitor set to 'sRGB' mode with a luminance range from $0.1 cdm^{-2}$ to $175 cdm^{-2}$, with spatial and temporal resolutions of 1920 by 1080 pixels and 60 Hz. The display was viewed at a distance of approximately 70 cm so that 40 pixels subtended 1 degree of visual angle. The full display subtended 49 by 27.5 degrees. The decoding nonlinearity of the monitor was recorded using a Konica Minolta LS 100 photometer and was found to be closely approximated by a gamma function with an exponent of 2.2. Stimuli were generated under Ubuntu 15.04 LTS running MATLAB (MathWorks) with functions from the Psychtoolbox [6, 42]. The experiment was conducted in a dark room.

4.3.3 Stimuli

30 randomly selected images were taken from the FADE dataset [11]. Dehazed versions of the original images were produced according to the proposed approach with $k = 0.4$ and the approaches of Choi *et al.* [11], Meng *et al.* [33], Tarel *et al.* [51], the Dark-Channel (DC) [21], and Wang *et al.* [56].

Ours	Tarel *et al.*	Meng *et al.*	Dark Channel	Choi *et al.*	Wang *et al.*
0.32	-0.29	-0.31	0.21	0.11	-0.05

Table 3: *Results for the psychophysical experiment using the Thurstone Case V analysis. The larger the value, the better the method.*

4.3.4 Procedure

The dehazed images were viewed on either sides of the original hazy image. Subjects were asked to select the image that they prefered out of the three displayed images. Given the 30 hazy images and 6 dehazed versions for each image, the total number of comparisons was 450. So, the experiment was conducted in 2 sessions and the subjects had unlimited time to make the choice. On average, it took around 25 minutes for each session.

4.3.5 Analysis of the results

The first analysis of our results shows that in 52% of the cases observers preferred the original image, instead of any of the two image processing solutions. This shows that there is still a long way to go regarding the development of new image dehazing methods capable of producing results pleasant to human observers. This result is in agreement with the work of Ma *et al.* [31], where the Mean Opinion Scores obtained by the original hazy images were similar to those obtained by different dehazing algorithms.

We have also analyzed the result of our experiment in terms of the Thurstone Case V Law of Comparative Judgment. To this end, we have converted our data into a pure pairwise comparison setting. We have done so by assigning 1 to an image processing method in case it was selected among the three images, and giving 0.5 for each method in the case the original hazy image was selected. The results for this setting are shown in Table 3, where we can see that our method is the one selected more often, followed by the Dark Channel, and the method by Choi *et al.*

The results presented in this subsection when compared with the results obtained from the quantitative metrics (Tables 1 and 2) indicate the importance of working towards defining better metrics for the image dehazing problem that are able to predict the users' preference.

4.4 Comparison versus other artifact-aware methods

Figure 9 presents a comparison of our results versus the artifact-aware methods of Chen *et al.* [10] and Li *et al.* [26]. From left to right we have the original image, the result of Li *et al.*, the result of Chen *et al.* and our result with $k = 0.4$. In these images we can clearly see that the method of Li *et al.* still presents color artifacts. These color artifacts come from the fact that this method aims to reduce blocking artifacts coming from compression, but it is still based on undoing Kochsmieder' law, and it therefore inherits the problems related to Eq.(4). On the other hand, the method of Chen *et al.* does not produce color artifacts. However, the results look cartoonish due to its dependence on a minimization based on total variation

Fig. 9: *Comparison versus other artifact-free methods. From left to right: Original, Li* et al. *[26], Chen* et al. *[10], and our method with* $k = 0.4$

which makes it prone to stair-casing artifacts. This is clearly visible on the building of the first image, the letters of the second image, or the tree in the third one.

4.5 Computational time

We compare in Table 4 the computational time of our non-optimized, non-parallelized implementation versus that of Wang *et al.* (using the authors' implementation) on Matlab R2015b in an Intel Core i7-3770 @ 3.40Ghz with 16Gb of RAM, and to other already published computational times for state-of-the-art methods run under a very similar computer configuration (16Gb and 3.50Ghz) for an image of size 720×580 [27]. In this table, we can see that our method is twice as fast as any of the other state-of-the-art methods.

We have also optimized and parallelized our algorithm using the CUDA platform. In this implementation the color conversions are approximated via look-up tables (LUT). The running time of our algorithm in a Nvidia Titan XP for a FullHD image (i.e. an image of size 1920×1080) is 90 milliseconds, which represents a time two orders of magnitude shorter than that of current state-of-the-art methods.

Method	Time (seconds)
Ancuti and Ancuti [1]	3.0
Tan [47]	3.3
Fattal [14]	141.1
He *et al.* [21]	20
Tarel *et al.* [51]	12.8
Kratz and Nishino [39]	124.2
Meng *et al.* [33]	**1.0**
Fattal [15]	1.9
Berman *et al.* [5]	1.8
Tang *et al.* [49]	10.4
Cai *et al.* [8]	**1.7**
Wang *et al.* [56]	43.4
Ours-$k = 0.4$ (only global)	**0.45 (0.40)**
Ours-$k = 0.4$ on GPU and FullHD	**0.09**

Table 4: *Comparison of run-time among the different methods in an image 720 x 580. Best time is marked in green, second-best in blue, and third-best in orange. The last row presents the result of our GPU implementation in a FullHD* 1920×1080 *image.*

Finally, let us note that for a color image of size 4000×3000, which is not tractable by many current methods due to its extremely large size, our non-optimized, non-parallelized Matlab version on the computer stated above has an approximate running time of 4.3 seconds. The same image, using our GPU implementation, has a running time of 300 milliseconds.

5 Summary and further work

In this work we have presented an image dehazing method whose main characteristics are to be artifact-free, based on human perception principles, independent from any physical constraint, and fast. To this end, we have worked in the HSV color space. Our proposed method first reduces the Value component with a global function that performs a constrained histogram flattening. Next, it replaces the Saturation component by keeping the colorfulness of the original image. Finally, local enhancement is applied to the Value component. Results show that our method competes with the state-of-the-art for standard images, and that it outperforms current methods when dealing with challenging images.

As further work, we would like to define a metric that is able to predict the preference of the users in our experiment, and to later look for the parameters of our approach that better minimize the newly defined metric.

6 Acknowledgments

This work was supported by the European Research Council, Starting Grant ref. 306337; by the European Unions Horizon 2020 research and innovation programme under grant agreements ref. 761544 and ref. 780470; by the Spanish government and FEDER Fund, grant ref. TIN2015-71537-P(MINECO/FEDER,UE); and by the Icrea Academia Award. JVC was supported by the Spanish government, grant ref. IJCI-2014-19516. The NVIDIA Titan X used for this research was donated by the NVIDIA corporation.

References

1. Ancuti, C., Ancuti, C.: Single Image Dehazing by Multi-Scale Fusion. IEEE Transactions on Image Processing **22**(8), 3271–3282 (2013)
2. Ancuti, C.O., Ancuti, C., Hermans, C., Bekaert, P.: A Fast Semi-inverse Approach to Detect and Remove the Haze from a Single Image. No. 6493 in Asian Conference on Computer Vision, ACCV-2010, pp. 501–514 (2010)
3. Ancuti, C., Ancuti, C.O., De Vleeschouwer, C.: D-hazy: A dataset to evaluate quantitatively dehazing algorithms. In: IEEE International Conference on Image Processing (ICIP), ICIP'16 (2016)
4. Bai, L., Wu, Y., Xie, J., Wen, P.: Real time image haze removal on multi-core dsp. Procedia Engineering **99**, 244 – 252 (2015). DOI https://doi.org/10.1016/j.proeng.2014.12.532. URL http://www.sciencedirect.com/science/article/pii/S1877705814036467. 2014 Asia-Pacific International Symposium on Aerospace Technology, APISAT2014 September 24-26, 2014 Shanghai, China
5. Berman, D., Treibitz, T., Avidan, S.: Non-local image dehazing. In: IEEE Conference on Computer Vision and Pattern Recognition (CVPR) (2016)
6. Brainard, D.H.: The psychophysics toolbox. Spatial vision **10**, 433–436 (1997)
7. Brenner, N., Bialek, W., de Ruyter van Steveninck, R.: Adaptive rescaling maximizes information transmission. Neuron **26**(3), 695 – 702 (2000). DOI http://dx.doi.org/10.1016/S0896-6273(00)81205-2. URL http://www.sciencedirect.com/science/article/pii/S0896627300812052
8. Cai, B., Xu, X., Jia, K., Qing, C., Tao, D.: DehazeNet: An End-to-End System for Single Image Haze Removal. arXiv:1601.07661 (2016). URL http://arxiv.org/abs/1601.07661
9. Carandini, M., Heeger, D.J.: Normalization as a canonical neural computation. Nature Reviews Neuroscience (1), 51–62 (2011). DOI 10.1038/nrn3136
10. Chen, C., Do, M.N., Wang, J.: Robust image and video dehazing with visual artifact suppression via gradient residual minimization. In: Computer Vision - ECCV 2016 - 14th European Conference, pp. 576–591 (2016). DOI 10.1007/978-3-319-46475-6_36. URL http://dx.doi.org/10.1007/978-3-319-46475-6_36
11. Choi, L.K., You, J., Bovik, A.C.: Referenceless Prediction of Perceptual Fog Density and Perceptual Image Defogging. IEEE Transactions on Image Processing **24**(11), 3888–3901 (2015)
12. Cyriac, P., Kane, D., Bertalmío, M.: Perceptual dynamic range for in-camera image processing. In: British Machine Vision Conference (BMVC) (2015)
13. El-Hashash, M.M., Aly, H.A.: High-speed video haze removal algorithm for embedded systems. Journal of Real-Time Image Processing (2016). DOI 10.1007/s11554-016-0603-1. URL https://doi.org/10.1007/s11554-016-0603-1
14. Fattal, R.: Single Image Dehazing. In: ACM SIGGRAPH 2008 Papers, SIGGRAPH '08, pp. 72:1–72:9. ACM, New York, NY, USA (2008)
15. Fattal, R.: Dehazing using Color-Lines. In: ACM Transaction on Graphics. ACM, New York, NY, USA (2014)
16. Galdran, A., Vazquez-Corral, J., Pardo, D., Bertalmío, M.: Enhanced Variational Image Dehazing. SIAM Journal on Imaging Sciences **8**(3), 1519–1546 (2015)
17. Galdran, A., Vazquez-Corral, J., Pardo, D., Bertalmío, M.: Fusion-based Variational Image Dehazing. IEEE Signal Processing Letters **24**(2), 151–155 (2017)
18. Galdran, A., Alvarez-Gila, A., Bria, A., Vazquez-Corral, J., Bertalmío, M.: On the duality between Retinex and Image Dehazing. In: Computer Vision and Pattern Recognition (CVPR) (2018)
19. Gao, Y., Hu, H.M., Wang, S., Li, B.: A fast image dehazing algorithm based on negative correction. Signal Processing **103**, 380–398 (2014)
20. Hautière, N., Tarel, J.P., Aubert, D., Dumont, E.: Blind contrast enhancement assesment by gradient rationing at visible edges. Image Analysis & Stereology **27**(2), 87–95 (2011)
21. He, K., Sun, J., Tang, X.: Single Image Haze Removal Using Dark Channel Prior. IEEE Transactions on Pattern Analysis and Machine Intelligence **33**(12), 2341–2353 (2011)
22. Kastner, D.B., Baccus, S.A.: Insights from the retina into the diverse and general computations of adaptation, detection, and prediction. Current opinion in neurobiology **25**, 6369 (2014). DOI 10.1016/j.conb.2013.11.012. URL http://dx.doi.org/10.1016/j.conb.2013.11.012
23. Kopf, J., Neubert, B., Chen, B., Cohen, M., Cohen-Or, D., Deussen, O., Uyttendaele, M., Lischinski, D.: Deep Photo: Model-based Photograph Enhancement and Viewing. In: ACM SIGGRAPH Asia 2008 Papers, pp. 116:1–116:10. ACM, New York, NY, USA (2008)
24. Koschmieder, H.: Theorie der horizontalen Sichtweite: Kontrast und Sichtweite. Keim & Nemnich (1925)
25. Lai, Y.H., Chen, Y.L., Chiou, C.J., Hsu, C.T.: Single-Image Dehazing via Optimal Transmission Map Under Scene Priors. IEEE Transactions on Circuits and Systems for Video Technology **25**(1), 1–14 (2015)

26. Li, Y., Guo, F., Tan, R.T., Brown, M.S.: A contrast enhancement framework with jpeg artifacts suppression. In: ECCV 2014: 13th European Conference, pp. 174–188 (2014). DOI 10.1007/978-3-319-10605-2_12. URL http://dx.doi.org/10.1007/978-3-319-10605-2_12
27. Li, Y., You, S., Brown, M.S., Tan, R.T.: Haze visibility enhancement: A survey and quantitative benchmarking. Computer Vision and Image Understanding **165**, 1 – 16 (2017). DOI https://doi.org/10.1016/j.cviu.2017.09.003. URL http://www.sciencedirect.com/science/article/pii/S1077314217301595
28. Li, Z., Zheng, J.: Edge-Preserving Decomposition-Based Single Image Haze Removal. IEEE Transactions on Image Processing **24**(12), 5432–5441 (2015)
29. Lissner, I., Preiss, J., Urban, P., Lichtenauer, M.S., Zolliker, P.: Image-difference prediction: From grayscale to color. IEEE Transactions on Image Processing **22**(2), 435–446 (2013). DOI 10.1109/TIP.2012.2216279
30. Luan, Z., Shang, Y., Zhou, Z, Shao, Z., Guo, G., Liu, X.: Fast single image dehazing based on a regression model. Neurocomputing **245**, 10–22 (2017)
31. Ma, K., Liu, W., Wang, Z.: Perceptual evaluation of single image dehazing algorithms. In: 2015 IEEE International Conference on Image Processing (ICIP), pp. 3600–3604 (2015). DOI 10.1109/ICIP.2015.7351475
32. Matlin, E., Milanfar, P.: Removal of haze and noise from a single image. In: Proc. SPIE 8296, Computational Imaging X, vol. 8296, pp. 82,960T–82,960T–12 (2012). DOI 10.1117/12.906773. URL http://dx.doi.org/10.1117/12.906773
33. Meng, G., Wang, Y., Duan, J., Xiang, S., Pan, C.: Efficient Image Dehazing with Boundary Constraint and Contextual Regularization. In: 2013 IEEE International Conference on Computer Vision (ICCV), pp. 617–624 (2013)
34. Mittal, A., Soundarajan, R., Bovik, A.C.: Making a completely blind image quality analyzer. IEEE Signal Processing Letters **22**(3), 209–212 (2013)
35. Mittal, A., Moorthy, A.K., Bovik, A.C.: No-reference image quality assessment in the Spatial Domain. IEEE Transactions on Image Processing **21**(12), 4695–4708 (2012)
36. Mizokami, Y., Takahashi, Y., Yaguchi, H.: Colorfulness perception of natural images adjusting to haze. In: The 23rd Symposium of the International Colour Vision Society (2015)
37. Mizokami, Y., Takahashi, Y., Yaguchi, H.: Stable colorfulness perception of scene through haze. In: Vision Sciences Society (VSS) (2016)
38. Narasimhan, S., Nayar, S.: Contrast restoration of weather degraded images. IEEE Transactions on Pattern Analysis and Machine Intelligence **25**(6), 713–724 (2003)
39. Nishino, K., Kratz, L., Lombardi, S.: Bayesian Defogging. International Journal of Computer Vision **98**(3), 263–278 (2012)
40. Oakley, J., Bu, H.: Correction of Simple Contrast Loss in Color Images. IEEE Transactions on Image Processing **16**(2), 511–522 (2007)
41. Olshausen, B.A., Field, D.J.: Vision and the coding of natural images. American Scientist **88**(3), 238–245 (2000)
42. Pelli, D.G.: The videotoolbox software for visual psychophysics: Transforming numbers into movies. Spatial vision **10**(4), 437–442 (1997)
43. Pizer, S.M., Amburn, E.P., Austin, J.D., Cromartie, R., Geselowitz, A., Greer, T., Romeny, B.T.H., Zimmerman, J.B.: Adaptive histogram equalization and its variations. Comput. Vision Graph. Image Process. **39**(3), 355–368 (1987). DOI 10.1016/S0734-189X(87)80186-X. URL http://dx.doi.org/10.1016/S0734-189X(87)80186-X
44. Schaul, L., Fredembach, C., Susstrunk, S.: Color image dehazing using the near-infrared. In: 2009 16th IEEE International Conference on Image Processing (ICIP), pp. 1629–1632 (2009)
45. Schechner, Y., Narasimhan, S., Nayar, S.: Instant dehazing of images using polarization. In: IEEE Computer Society Conference on Computer Vision and Pattern Recognition. CVPR 2001, vol. 1, pp. I–325–I–332 vol.1 (2001)
46. Sun, W.: A new single-image fog removal algorithm based on physical model. Optik - International Journal for Light and Electron Optics **124**(21), 4770–4775 (2013)
47. Tan, R.: Visibility in bad weather from a single image. In: IEEE Conference on Computer Vision and Pattern Recognition, 2008. CVPR 2008, pp. 1–8 (2008)
48. Tang, K., Yang, J., Wang, J.: Investigating Haze-Relevant Features in a Learning Framework for Image Dehazing. In: 2014 IEEE Conference on Computer Vision and Pattern Recognition (CVPR), pp. 2995–3002 (2014)
49. Tang, K., Yang, J., Wang, J.: Investigating haze-relevant features in a learning framework for image dehazing. In: 2014 IEEE Conference on Computer Vision and Pattern Recognition, pp. 2995–3002 (2014). DOI 10.1109/CVPR.2014.383

50. Tarel, J.P., Hautiere, N.: Fast visibility restoration from a single color or gray level image. In: 2009 IEEE 12th International Conference on Computer Vision, pp. 2201–2208 (2009)
51. Tarel, J.P., Hautiere, N., Caraffa, L., Cord, A., Halmaoui, H., Gruyer, D.: Vision Enhancement in Homogeneous and Heterogeneous Fog. IEEE Intelligent Transportation Systems Magazine **4**(2), 6–20 (2012)
52. Tarel, J.P., Hautiere, N., Cord, A., Gruyer, D., Halmaoui, H.: Improved visibility of road scene images under heterogeneous fog. In: 2010 IEEE Intelligent Vehicles Symposium (IV), pp. 478–485 (2010)
53. Vazquez-Corral, J., Zamir, S., Galdran, A., Pardo, D., Bertalmío, M.: Image processing applications through a variational perceptually-based color correction related to retinex. In: IS&T Electronic Imaging Conference (2016)
54. Wan, Y., Chen, Q.: Joint image dehazing and contrast enhancement using the hsv color space. IEEE International Conference on Visual Communications and Image Processing (2015)
55. Wang, J.B., He, N., Zhang, L.L., Lu, K.: Single image dehazing with a physical model and dark channel prior. Neurocomputing **149, Part B**, 718–728 (2015)
56. Wang, S., Cho, W., Jang, J., Abidi, M.A., Paik, J.: Contrast-dependent saturation adjustment for outdoor image enhancement. J. Opt. Soc. Am. A **34**(1), 7–17 (2017). DOI 10.1364/JOSAA.34.000007. URL http://josaa.osa.org/abstract.cfm?URI=josaa-34-1-7
57. Wang, W., Yuan, X.: Recent advances in image dehazing. IEEE/CAA Journal of Automatica Sinica **4**(3), 410–436 (2017)
58. Wang, W., Yuan, X., Wu, X, Liu, Y.: Dehazing images with a large sky region. Neurocomputing **238**, 365–376 (2017)
59. Wang, W., Yuan, X., Wu, X, Liu, Y.: Fast Image Dehazing Method Based on Linear Transformation. IEEE Transactions on Multimedia **19**(6), 1142–1155 (2017)
60. Wang, Y., Wang, H., Yin, C., Dai, M.: Biologically inspired image enhancement based on Retinex. Neurocomputing **177**, 373–384 (2016)
61. Yoon, I., Kim, S., Kim, D., Hayes, M.H., Paik, J.K.: Adaptive defogging with color correction in the hsv color space for consumer surveillance system. IEEE Trans. Consumer Electronics **58**(1), 111–116 (2012). URL http://dblp.uni-trier.de/db/journals/tce/tce58.html#YoonKKHP12
62. Zhang, X.S., Gao, S.B., Li, C.Y., Li, Y.J.: A Retina Inspired Model for Enhancing Visibility of Hazy Images. Frontiers in Computational Neuroscience p. 151 (2015)
63. Zhu, Q., Mai, J., Shao, L.: A Fast Single Image Haze Removal Algorithm Using Color Attenuation Prior. IEEE Transactions on Image Processing **24**(11), 3522–3533 (2015)

Appendix: sRGB/HSV color conversions

From sRGB to HSV

Given a pixel (R, G, B) in sRGB space, we start by defining $M = max(R, G, B)$ and $m = min(R, G, B)$. Let us also define an auxiliary variable H' in the following way

$$H' = \begin{cases} 0 & \text{if } M - n = 0. \\ \frac{G-B}{M-m} \mod 6 & \text{if } M = R. \\ \frac{B-R}{M-m} + 2 & \text{if } M = G. \\ \frac{R-G}{M-m} + 4 & \text{if } M = B. \end{cases} \tag{9}$$

Then, the HSV coordinates are defined as

$$H = H' \times 360. \tag{10}$$

$$S = \frac{M - m}{M}. \tag{11}$$

$$V = M. \tag{12}$$

From HSV to sRGB

Given a pixel (H, S, V) in the HSV space we start by defining $C = S \times V$, $H' = \frac{H}{60}$, $X = C \times (1 - \|H' \mod 2 - 1\|)$, and $m = V - C$. Then the pixel value in sRGB color space is defined as

$$(R, G, B) = \begin{cases} (m, m, m) & \text{if } C = 0. \\ (C + m, X + m, m) & \text{if } 0 \leq H' \leq 1. \\ (X + m, C + m, m) & \text{if } 1 \leq H' \leq 2. \\ (m, C + m, X + m) & \text{if } 2 \leq H' \leq 3. \\ (m, X + m, C + m) & \text{if } 3 \leq H' \leq 4. \\ (X + m, m, C + m) & \text{if } 4 \leq H' \leq 5. \\ (C + m, m, X + m) & \text{if } 5 \leq H' \leq 6. \end{cases} \tag{13}$$